Reexamining the Lyman-Birge-Hopfield band of N_{2}

J. A. Bradley, A. Sakko, G. T. Seidler, A. Rubio, M. Hakala, K. Hämäläinen, G. Cooper, A. P. Hitchcock, K. Schlimmer, and K. P. Nagle

Phys. Rev. A **84**, 022510 — Published 23 August 2011

DOI: 10.1103/PhysRevA.84.022510

Revisiting the Lyman-Birge-Hopfield Band of N_2

by J.A. Bradley[1,2,*], A. Sakko[3], G.T. Seidler[2], A. Rubio[4], M. Hakala[3], K. Hämäläinen[3], G. Cooper[5], A.P. Hitchcock[5], K. Schlimmer[2], K.P. Nagle[2]

1. Condensed Matter and Materials Division, Lawrence Livermore National Laboratory, Livermore, CA 94550
2. Physics Department, University of Washington, Seattle, WA 98195
3. Department of Physics, FI-00014, University of Helsinki, Finland
4. Nano-Bio Spectroscopy Group and ETSF Scientific Development Center, Dpto. Física de Materiales, Universidad del País Vasco, Centro de Física de Materiales CSIS-UPV/EHU-MPC and DIPC, Av. Tolosa 72, E-20018 San Sebastián, Spain
5. Brockhouse Institute for Materials Research, McMaster University, Hamilton, Ontario, Canada L8S 4M1

Motivated by fundamental molecular physics and by atmospheric and planetary sciences, the valence excitations of N_2 gas have seen several decades of intensive study, especially by electron energy loss spectroscopy (EELS). It was consequently surprising when a comparison of nonresonant inelastic x-ray scattering (NIXS) and nonresonant EELS found strong evidence for violations of the first Born approximation for EELS when leaving the dipole scattering limit. Here we reassess the relative strengths of the constituent resonances of the lowest energy excitations of N_2, encompassed by the so-called Lyman-Birge-Hopfield (LBH) band, by expanding on the prior, qualitative, interpretation of the NIXS results for N_2 by both quantifying the GOS of the lowest-energy excitations and also presenting a new time-dependent density functional theory calculation of the *q*-dependence of the entire low-energy electronic excitation spectrum. At high *q*, we find that the LBH band has an unexpectedly large contribution from the octupolar $w^1\Delta_u$ resonance exactly in the regime where theory and EELS experiment for the presumed-dominant $a^1\Pi_g$ resonance have previously had substantial disagreement, and also where the EELS results must now be expected to show violations of the first Born approximation. After correcting for this contamination, the $a^1\Pi_g$ GOS from the NIXS results is in good agreement with prior theory. The NIXS spectra, over their entire *q* range, also find satisfactory agreement with the new TDDFT calculations for both bound and continuum excitations.

*corresponding author: bradley41@llnl.gov

Keywords: Lyman-Birge-Hopfield, nitrogen valence excitation, inelastic x-ray scattering

PACS: 33.20.Rm, 31.15.A-. 34.50.Gb

Submitted Physical Review A 30 March, 2011

I. **Introduction**

The excited state electronic structure of atomic, molecular, and condensed phases necessarily includes states with a great diversity of local symmetries, including states that are not coupled to the ground state by electric dipole transitions. Unfortunately, photon absorption measurements are typically constrained by the dipole selection rule ($\Delta l = 1$). Photon absorption studies therefore give an incomplete characterization of the excited state electronic structure. For many systems, particularly those of high symmetry, a range of selection rules need be accessed to fully characterize and understand the system.

In contrast, nonresonant inelastic x-ray scattering (NIXS) is an emergent technique for understanding local electronic structure [1-21] exhibiting more flexibility in transition selection rules and hence sensitivity to a more diverse set of final states. The double-differential cross-section (DDCS) for NIXS is

$$\frac{d^2\sigma}{d\Omega d\omega} = \left(\frac{d\sigma}{d\Omega}\right)_{Th} S(\mathbf{q},\omega) \quad (1)$$

where

$$S(\mathbf{q},\omega) = \sum_f \left|\left\langle u_f \left| e^{i\mathbf{q}\cdot\mathbf{r}} \right| u_i \right\rangle\right|^2 \delta(E_f - E_i - \hbar\omega) \quad (2)$$

is known as the *dynamic structure factor* and $\left(\frac{d\sigma}{d\Omega}\right)_{Th}$ is the Thomson cross-section. In Eqs. 1 and 2, $\hbar\boldsymbol{q}$ and $\hbar\omega$ are the momentum and energy transfers, u_i *and* u_f refer to the initial and final quasiparticle states, respectively, and E_i and E_f are their energies. NIXS has primarily been applied to condensed phase systems, but recent work has shown its applicability to atomic and molecular systems. This was seen in the preliminary, instrument-driven work of Minzer, et al., on two-electron excitations in He [22], in the

very careful study of the $1s \rightarrow 2s$ and $1s \rightarrow 2p$ excitation in He by Xie, *et al*. [23], and in the study of the valence-level, localized excitations of N_2 by Bradley, *et al* [1].

As with traditional x-ray absorption spectroscopies, NIXS results are most valuable in conjunction with appropriate theoretical treatment. This has been demonstrated in weakly correlated condensed phase systems with the use of multiple scattering [24-26] and density functional [27-28] techniques, and in strongly correlated systems with the application of atomic multiplet theory [3, 29] and density functional methods [30]. New theoretical treatments of molecular systems at a reasonable computational cost are very valuable, and they can now be directly compared against the comprehensive interrogation of electronic structure provided by NIXS. In this work we present such a comparison, using a time dependent density functional theory (TDDFT) treatment. We predict the electronic structure of gas phase N_2 and use the predictions to analyze the NIXS results first reported by Bradley, *et al* [1]. This new pairing of theory and experiment for molecular systems is shown to provide key insights in the case of N_2, correcting prior ambiguities about symmetries of the bound excited states and demonstrating improved agreement between theory and experiment in the limit of high momentum transfer.

In particular, we use the measurements (by both EELS and NIXS) from Bradley et al. [1] together with new TDDFT calculations, all presented in absolute units, to quantitatively investigate the Lyman-Birge-Hopfield (LBH) resonance band of N_2 as a function of momentum transfer. The LBH band includes the three lowest energy singlet electronic excitations of N_2 and has seen decades of study [31-46]. The properties of the LBH band have been pursued both for fundamental reasons and also because of its

importance for atmospheric electricity and optical emission for the Earth and the moons Titan and Triton [31, 47-49]. The high-energy, *i.e.*, nonresonant excitation of the LBH band has been used as a testing ground for electronic structure theory [35, 50-51] and as a benchmark standard for comparison across numerous *q*-dependent nonresonant EELS spectrometers constructed for gas phase studies [32, 36, 41, 52], starting with the earliest measurements of Lassettre [40]. Here, we revisit the nonresonant excitation of the LBH band. We find two important details that have not previously been discussed. Specifically, prior determinations of the high-*q* generalized oscillator strength (GOS) of the main, $a^1\Pi_g$ contributor to the LBH band have been contaminated with significant weight from the neighboring $w^1\Delta_u$ resonance, and have also been outside of the first Born approximation, *i.e.*, have been in a kinematic regime where the EELS analogy to Eq. 1 does not hold, contrary to the assumptions built into theoretical treatment of these spectra [50].

The conclusions regarding the $w^1\Delta_u$ resonance are motivated by the experimental *q*-dependence of the line-shape and central location of the LBH band, along with the *q*-dependence of the extracted generalized oscillator strength (GOS) from the NIXS and EELS experiments and TDDFT calculations. Our *ab initio* calculations agree well with experiments despite the difficulties posed by the highly correlated electrons in the N-N triple bond. Our experimental and theoretical results also suggest an important path forward. Improved energy resolution (i.e., ~30 meV resolution) NIXS studies would allow measurements to resolve vibrational excitations, yielding a new spectroscopic approach to molecular electronic structure and bonding, both in the ground and the excited states. Given the applicability of Eq. 1 for nonresonant inelastic x-ray scattering,

NIXS may become a preferred experimental testing ground for excited state electronic properties in atomic and molecular systems. [1, 17, 18]

The paper continues as follows. First, in section II, we summarize experimental methods. This section emphasizes the treatment of the NIXS and EELS results of Bradley, et al., [1] for absolute normalization of $S(q,\omega)$ and determination of the q-dependent GOS of the LBH band. One general point that arises in this section is the complete statistical independence of sources of systematic error in the respective NIXS and EELS studies. Second, in section III, we summarize theoretical methods. This includes an outline of the steps taken to implement the TDDFT formalism both in the energy regimes of bound excitations and the continuum for N_2, in addition to commenting on methods for extracting the GOS for the different resonances that make up the LBH band. In section IV we present and compare our experimental and theoretical results. We compare NIXS, EELS, and TDDFT in terms of $S(q,\omega)$ and GOS. We discuss and explain previously unreported q-dependence of the line-shape and central location of the LBH band at ~ 1eV resolution. Finally, in section V we conclude and give our outlook for the future developments and applications of the presented methodology.

II. Experimental Methods

Part of the NIXS and EELS results used in this work were first reported elsewhere [1]. The novel experimental details to be presented here are the normalizations of the NIXS and EELS results to obtain $S(q,\omega)$ in absolute units, together with the consequent determination and uncertainty estimates for the q-dependent generalized oscillator

strength (GOS). Following the practice of prior work in the field [53], $S(q,\omega)$ for both the NIXS and EELS data were placed into units of eV^{-1}.

For NIXS, the spectra were placed into absolute units by application of the Bethe *f*-sum rule [53]. In our notation and in atomic units, this rule states that

$$N = \frac{2}{q^2}\int_0^\infty \omega S(q,\omega)\, d\omega, \quad (3)$$

where N is the number of electrons in the system probed (for N_2, N=14). Eq. 1 can be solved to give $S(q,\omega)$ in terms of the NIXS DDCS, so the process of placing the spectra into real units is tantamount to integration of a measured quantity. Namely, the measured spectra were rescaled to enforce

$$N = \frac{2}{q^2}\int_0^\infty \omega\left(\frac{d\sigma}{d\Omega}\right)_{Th}^{-1}\frac{d^2\sigma}{d\Omega d\omega}. \quad (4)$$

Because of the sum rule, Eq. 3 provides a unitless way to determine the strength of the excitation character of a given spectral feature. This metric is called the Generalized Oscillator Strength (GOS), and for an excitation isolated in the energy range between ω_1 and ω_2 it is

$$GOS(q) = \frac{2}{q^2}\int_{\omega_1}^{\omega_2} \omega S(q,\omega) d\omega. \quad (5)$$

In practice, because of overlapping spectral features, GOS is typically determined by fitting the dynamic structure factor by e.g. Gaussians and integrating the fitted function. While the $1/q^2$ dependence can mask subtle spectral deviations between theory and experiment at high momentum transfer, we will use it here to make best contact with prior work of the gas-phase EELS community.

We now discuss the implementation of Eq. 3 with experimental data. A typical wide energy range NIXS scan is presented in Figure 1. A systematic, weak background—linear in incident energy—was determined by a measurement with the sample removed from the path of the beam. The background was then removed by fitting a linear function between such scans (taken at energies below and above the region of interest—see Figure 1) and subtracting the result from the data. The data were shifted to units of energy loss, rather than incident photon energy, using the position of the elastic peak [2, 54-55]. At highest energy, where $S(q,\omega)$ is very small, statistical fluctuations in the background numerically destabilize the integral in Eq. 3, so the high-energy tails of the spectra were fit to a smoothly decaying functional form ($1/\omega^3$, see Figure 1, inset). At high energy loss, these forms were used in the integral in place of the data.

The final errors in the overall NIXS spectral normalization to absolute units are 10%. The main contributors to this error schedule are as follows. The reliability of corrections for the energy dependence of the incident-beam monitors provide 3.5%. Corrections for the weak background provide an additional 5.5% error, determined by variation of the background fitting procedure. The use of a fixed-detector geometry requires that q is a weak function of incident energy, thus complicating application of the Bethe *f*-sum rule. Comparing single analyzer spectra with spectra interpolated between detectors in order to fix q indicates an error of 4.0%, peaked at higher q analyzers. An additional 6.5% error comes from uncertainties in the shape of the very high-energy tail of the Compton scattering profile, determined by performing the integral with and without the smooth high-energy fit. We find that these errors are largely uncorrelated,

and consequently add them in quadrature to reach the final error estimate for spectra at each q.

Absolute electron energy loss spectra double differential cross section (DDCS) were obtained by normalizing the measured elastic scattering peak intensity to the published N_2 elastic electron scattering cross-section [56] at each scattering angle. The spectra being analyzed here for the LBH GOS are again the same as from Bradley, et al [1]. The EELS $S(\mathbf{q},\omega)$ was then derived by inverting

$$\left(\frac{d^2\sigma}{d\Omega d\omega}\right)_{EELS} = \left(\frac{d\sigma}{d\Omega}\right)_{Ru} S(\mathbf{q},\omega) \quad (6)$$

subject to the known Rutherford cross-section, $\left(\frac{d\sigma}{d\Omega}\right)_{Ru}$. This relation holds when the scattering follows the first Born approximation. While this was shown to be invalid at moderate to high momentum transfer [1], removal of the Rutherford cross section to reach an effective $S(\mathbf{q},\omega)$ allows for a quantitative comparison with NIXS and theory. Determination of the LBH GOS inherits the normalization uncertainty discussed above, but also at low q, the tail of the elastic scattering peak overlaps the LBH feature. The fitting and removal of this feature, along with the removal of the dipole-allowed resonances at ~13eV, create additional uncertainty.

Final uncertainties in the NIXS LBH GOS estimate range from 12% to 20% (from high to low q, respectively), and are included in the presentation of the data (see Figures 6-7, as discussed in section IV, below). It is important to note that the normalizations to absolute units for NIXS (using the *f*-sum rule) and the EELS (using normalization to accepted standard values of the elastic scattering cross-section) are fully independent.

Consequently, the NIXS and EELS techniques have strongly independent systematic errors regarding both instrumentation and data analysis.

III. Theoretical Methods

Theoretical dynamic structure factor and GOS curves for the valence excitations of N_2 were calculated using time-dependent density functional theory (TDDFT) which has provided widely used computational methods for simulating excited state properties, such as the dielectric response, of materials [57]. It has become very popular due to its high accuracy versus computational efficiency. In this work we employed the real-space computer code Octopus [58] and its recently developed feature for calculating the dynamic structure factor within TDDFT [59]. The GOS curves for LBH-related transitions were calculated using Casida's equation that provides transition energies as a solution to a matrix equation that couples the different single-electron excitations [60]. The generalized oscillator strengths are calculated from the eigenvectors of Casida's equation.

The above method is efficient for simulating bound-to-bound transitions in small molecules, but at wider energy range the IXS spectra were calculated using an alternative TDDFT scheme, namely the time-propagation method [61]. In this approach the electronic structure of the molecule is evolved in time under an influence of an external field $V_{ext}(\mathbf{r},t) = I_0 e^{i\mathbf{q}\cdot\mathbf{r}}\delta(t)$, and the induced fluctuations of charge density describe the response of the system to this perturbation. The IXS spectrum is obtained by Fourier transformation of the induced charge density [59].

The experimental N-N bond length of 1.098 Å was used in our calculations. Norm-conserving Troullier-Martins pseudopotentials were employed, and exchange and correlation were included within adiabatic local density approximation (ALDA). For calculating the GOS curves, 60 unoccupied electronic states were used. The real-space grid was spherically shaped with a radius of 8.0 Å and the uniform spacing between grid points was 0.18 Å. Additionally in the time propagation calculations, to simulate excitations above ionization threshold, an absorbing layer of width 5.0 Å was added to the grid. The layer removes part of the excited electrons from the system and thus simulates ionization [62]. The time evolution was followed for 7 $\hbar / eV$ and the resulting spectra were convoluted by Gaussian lineshape (using the experimental resolution of 1 eV).

IV. Results and Discussion

In Figure 2, we present a key result of this paper: the comparison between $S(q,\omega)$ as derived from NIXS, EELS and TDLDA (TDDFT within ALDA) calculations, each presented in absolute units. TDLDA correctly predicts the features in the experimental spectra, and moreover exhibits sharp decay in all features for q above ~3 a.u., displaying agreement with NIXS results but not with the EELS results. In general, TDLDA is an excellent predictor of $S(q,\omega)$ derived from bound-state final states (energy loss <15eV). The general shape and structure of the continuum excitations are also well predicted. At higher energy loss, near to the binding energy of the N 2*s* electrons, the sharpness and relative intensity of the predicted $S(q,\omega)$ at high q is clearly overestimated. This is at least partly due to the fact that the calculation neglects the finite lifetime of the electronic excitations, as well as the effects from ion dynamics, i.e. vibrational

broadening and the possible nonradiative decay through photodissociation. Also the spurious self-interaction is known to obscure the TDLDA calculation of core-electron excitations due to their highly localized nature [63] and possibly the pronounced ($2s\sigma \rightarrow$LUMO) excitation exposes a similar problem here. The full analysis of the discrepancy between the experiment and calculation in this energy regime is an interesting topic for further work.

In Figure 3, we focus on the valence-level excitation spectrum of N_2 at a single momentum transfer—low enough that the agreement between EELS and NIXS is still good over large parts of the energy loss range [1]. Final states are identified by their accepted symmetry designations, and both non-resonant electron (for the present range of experimental parameters) and photon scattering are sensitive only to transitions to singlet final states. Electron scattering measurements, both non-resonant and resonant, of the dipole-forbidden excitation feature(s) at ~9 eV have a long history [31-46, 64], making this feature an obvious point of comparison for the gas phase NIXS and EELS.

Low incident energy EELS studies, where the scattering dynamics have long been known to be complex and the energy resolution is frequently high enough to resolve even vibrational sub-levels, have carefully addressed the existence of several final states ($a^1\Pi_g, a'^1\Sigma_u^-, w^1\Delta_u$) in the energy range of the LBH band (~7-10.5 eV) [34, 37-38, 45,47]. However, studies with higher energy incident electrons, which typically have much poorer energy resolution, have tended to downplay or ignore possible contributions to the measured spectra and the GOS due to the $w^1\Delta_u$ and $a'^1\Sigma_u^-$ final states; many such studies have instead identified this feature solely with the $a^1\Pi_g$ final state or simply referred to it as the "LBH band," with no attempt to separate the contribution from the

various resonances [36, 41-42, 44]. Given the complications to electron scattering at high momentum transfer, q-dependent NIXS provides a new capability for such a separation, the details of which we now discuss.

The dependence of $S(\mathbf{q},\omega)$ (and hence GOS) on the relevant selection rule for a bound state excitation follows from expanding the exponential operator of Eq. 2 in spherical harmonics. Performing a directional average appropriate for disordered, polycrystalline or gaseous samples [65], the experimental quantity of interest, $S(q,\omega)$, is seen to depend only on the length of the momentum transfer vector q

$$S(q,\omega) = \sum_{l,m} \left| 4\pi i^l \left\langle u_f \left| j_l(qr) Y_{lm}(\hat{\mathbf{r}}) \right| u_i \right\rangle \right|^2 . \quad (7)$$

The q-dependence is entirely in the spherical Bessel function. Since $j_l(qr) \to 0$ at order $(qr)^l$ as $qr \to 0$, we can make the following general statements: At low q, $S(q,\omega)$ shows dipole-allowed transitions (and any monopole transition intensity that survives the integral after imposing ground-state orbital orthogonality [65]). As q grows, these transitions fade away, and quadrupole transitions dominate $S(q,\omega)$. As q continues to grow, this process repeats at higher and higher multipoles: quadrupole transitions fading and octupole transitions rising, and so on [65-66].

We can discuss the $a^1\Pi_g$, $a'^1\Sigma_u^-$ and $w^1\Delta_u$ resonances in the context of such selection rules: $a^1\Pi_g$ is dipole-forbidden and quadrupole-allowed, since in terms of single electron orbitals it involves transitions from $3s\sigma_g$ to $2p\pi_g$, and both initial and final states are of even parity. The $a'^1\Sigma_u^-$ and $w^1\Delta_u$ features both involve transitions between $2p\pi_u$ and $2p\pi_g$ single electron orbitals, and $p \to p$ transitions are dipole

forbidden [67]. For quadrupole transitions, initial and final states must have the same parity, implying that the $a'^{1}\Sigma_u^-$ and $w^1\Delta_u$ are to lowest order octupole-allowed. Therefore, we expect $a^1\Pi_g$ to be visible at moderate q, giving way to $a'^{1}\Sigma_u^-$ and $w^1\Delta_u$ as q grows. These three electronic excitations have significant vibrational structure but their centroids are expected to be in the vicinity of 9.3 eV, 9.8 eV, and 10.2 eV, respectively [38, 68]. Given the vibrational broadening of the features and the width of the NIXS/EELS energy response functions, the selection rules would be visible as changes in the height and energy of a broad feature at ~9.5 eV.

In Figure 4, we present an enlarged view of the q-dependence of this spectral region in the EELS and NIXS results. These data immediately motivate our central observation: both the line-shape and the central energy of this feature evolve strongly with increasing q. Surveying prior work at sufficiently high q, [31-46, 64] this has not previously been noted; in fact, very few presentations of raw spectra (as opposed to integrated GOS(q) summaries) appear in the literature. Complications in the q-dependence of the vibrational structure (e.g. failure of the Franck-Condon approximation) are possible, but the observed line-shape evolution is more likely due to a strong contribution from the octupole-allowed $w^1\Delta_u$ state; this state would become measurable as the (quadrupole allowed-only) $a^1\Pi_g$ state weakens at sufficiently high q.

The $w^1\Delta_u$ hypothesis is strongly supported by our calculations. In Figure 5 we present a comparison between measured (NIXS) and predicted (TDLDA) S(q,ω) for N_2 in the LBH energy range. Note again the use of absolute units for all results presented. The calculation was performed for purely electronic transitions (i.e. ignoring vibrational

effects) and the result demonstrates the importance of at least two electronic-state resonances with different selection rules in this energy range. We also fit the NIXS data for the three possible spectral features in this energy range ($a^1\Pi_g$, $w^1\Delta_u$, and $a'^1\Sigma_u^-$), including the partitioning into vibrational levels as determined by Franck-Condon factors in the literature [38]. The feature at 13 eV and the tail of the elastic peak were included in the fitting procedure. In fitting to the experimental data, including the $a'^1\Sigma_u^-$ resonance gives little weight to this spectroscopic feature [34]. Based on this fact, on the energies derived from the fitting procedure, and on the *q*-dependence, we identify two underlying features: the $a^1\Pi_g$ and $w^1\Delta_u$ resonances. The negligible intensity of the $a'^1\Sigma_u^-$ resonance is expected also from the symmetry properties of the involved electronic states as described elsewhere [69], and although the TDDFT does not provide its excitation energy correctly, the calculated GOS for this feature is correctly zero. Also in Figure 5, we present the decomposition of the observed LBH band into these resonances for some characteristic *q*-values. Overall, the agreement between the TDLDA calculations and the full range of observed valence-level excitations is impressive, and suggests that this method may have broad application in molecular spectroscopy [59].

The spectral response, $S(q,\omega)$, can be turned into GOS and reported as a function of *q*, as discussed in terms of Eq. 5. The GOS quantity is the most often quoted experimental benchmark for EELS investigations into bound-state resonances such as the LBH. In Figure 6, the GOS results for the resonances in the LBH band, as measured by NIXS and EELS, are reported and compared to earlier EELS studies. Because earlier work reported the integrated GOS of the entire 9 eV spectral feature [19, 24-25, 27],

rather than breaking it into $a^1\Pi_g$, $w^1\Delta_u$ and $a'^1\Sigma_u^-$ components, the GOS of the total LBH band is similarly used for comparison of NIXS to prior EELS studies in Figures 6(a) and 6(b). The agreement between NIXS and current/prior EELS work is good up to q~3 a.u., where violations of the Born approximation begin to drive the EELS-derived GOS much higher, as is shown in the inset.

In Figure 7(a), the GOS of the $a^1\Pi_g$ and $w^1\Delta_u$ are plotted separately as a function of momentum transfer. In Figure 7(b), NIXS results are compared to previous calculations of the LBH GOS. Note that the calculation of Giannerini, et al. [50] predicts a sharp drop-off in GOS at high q (where $log_{10}(q^2) \sim 0.5$, or $q \sim 1.8$ a.u.). This prediction is in stark contrast to all previous EELS measurements, and also disagrees with the NIXS measurement of the GOS of the integrated LBH band. However, upon decomposition of the LBH band into $a^1\Pi_g$ and $w^1\Delta_u$ contributions, the likely explanation is evident here, just as it was in terms of $S(q,\omega)$: The GOS at higher q is pushed upward by the contribution of the octupole-allowed $w^1\Delta_u$ resonance.

Our calculations strongly support this explanation as well, as can be seen in Figure 7(c). The comparison of TDLDA and NIXS GOS decompositions shows excellent agreement, especially in terms of q-dependence, which is a straightforward measure of electronic excitation structure. Considering that the calculations do not include vibrational effects, the overall quantitative agreement is quite strong, especially for the $w^1\Delta_u$ feature. Note that the combination of EELS and TDLDA alone would not settle the line-shape question definitively, since the highest-q (~5.3 a.u.) EELS GOS is far

(~5x) greater than that of the NIXS and the TDLDA. This fact is evident in Figure 6(b) (inset), and in Figure 2—there in terms of $S(q,\omega)$.

V. Conclusions and Future Directions

In conclusion, we report a quantitative reinvestigation of the nonresonant excitation of the lowest-energy exitations of the N_2 molecule, namely those in the Lyman-Birge-Hopfield (LBH) band. Nonresonant inelastic x-ray scattering (NIXS) with the assuredly simple target-probe interaction, are shown to be an effective experimental comparison for time dependent density functional theory calculations on this important and difficult molecular system. Specifically, in this case the combination of NIXS and TDLDA was able to identify and explain effects on the LBH generalized oscillator strength caused by the influence of the unexpectedly-important $w^1\Delta_u$ resonance. After correcting for this contribution, the $a^1\Pi_g$ generalized oscillator strength is in improved agreement with previous theory. Our results show that the adiabatic local density approximation (ALDA) can be appropriate for simulating bound transitions in small molecules and future studies with the same framework but using more sophisticated exchange-correlation functionals could also tackle e.g. double excitations.

In this paper, we have exhibited a new connection between electronic structure theory and experiment that we feel has great current utility and future promise. The NIXS/TDDFT combination can be used as exhibited here to understand bound-state electronic excitation structure for arbitrary molecular systems. Furthermore, the coupling of high resolution NIXS and vibronically-informed TDDFT holds great promise for future studies of electronic and vibrational structure for a wide variety of gas-phase materials.

We thank Edward Kelsey, Don Madison, William McCurdy, Charles Malone, and Paul Johnson for useful discussions. This work was supported by the U.S. Department of Energy, the Natural Sciences and Engineering Research Council (NSERC) of Canada, the Australian Research Council, the Research Funds of the University of Helsinki and the Academy of Finland (Contract 1127462, Centers of Excellence Program 2006-2011, and National Graduate School in Materials Physics). PNC/XOR facilities at the Advanced Photon Source, and research at these facilities, are supported by the US Department of Energy - Basic Energy Sciences, a Major Resources Support grant from NSERC, the University of Washington, Simon Fraser University and the Advanced Photon Source. Use of the Advanced Photon Source is also supported by the U. S. Department of Energy, Office of Science, Office of Basic Energy Sciences, under Contract DE-AC02-06CH1135. AR acknowledges support by MICINN (FIS2010-21282-C02-01), ACI-promociona (ACI2009-1036), Grupos Consolidados UPV/EHU del Gobierno Vasco (IT-319-07), and the European Community through e-I3 ETSF project (Contract No. 211956)

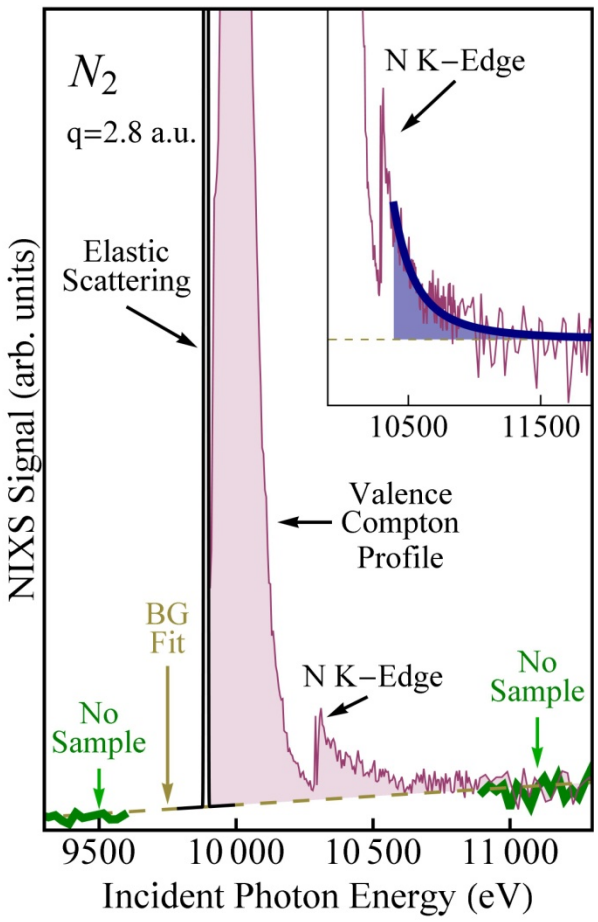

FIG. 1. (Color online) A NIXS scan for N_2 gas over a wide energy range (shaded). The fit to the instrumental background is shown (dashed), which is derived from high and low energy scans with the sample chamber removed and only He at 1 atmosphere in the beam-path (thick line). A mock elastic scattering response is included for visual orientation. The inset shows the high-energy tail of the same data with the instrumental background removed, and it displays the fit at high energy (thick line, shaded) that is used to stabilize the *f*-sum normalization integral.

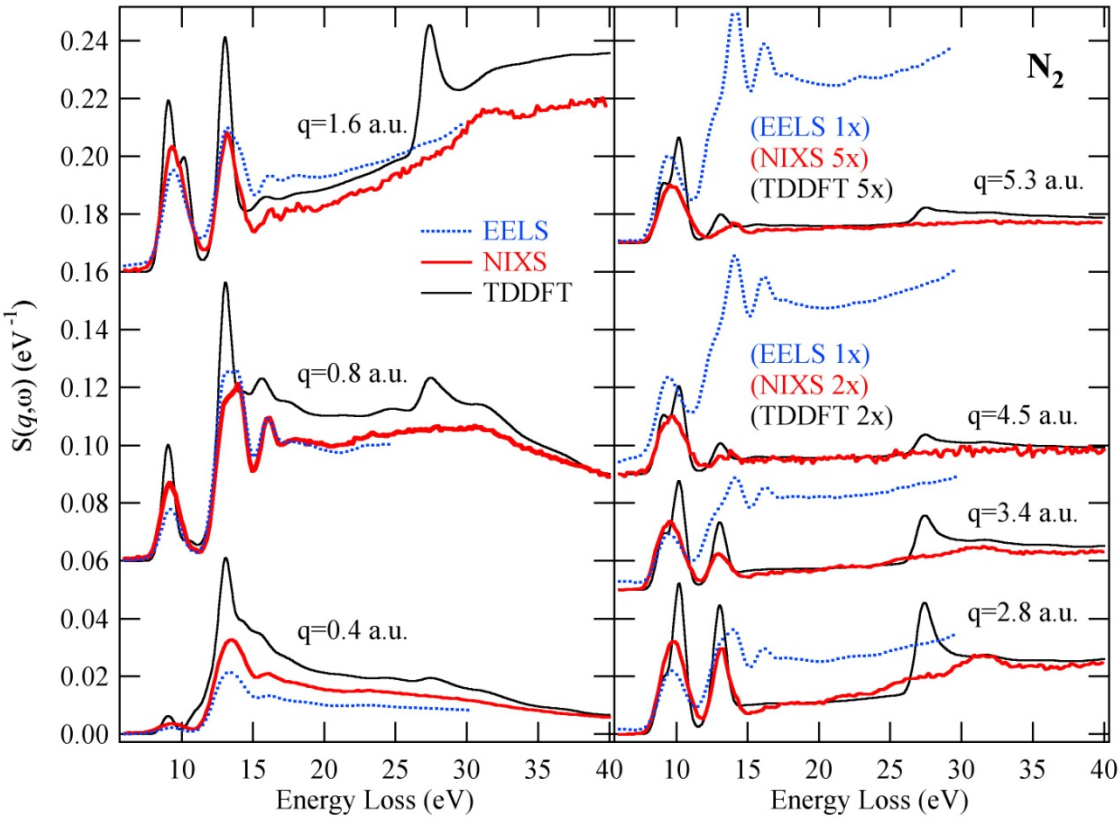

FIG. 2. (Color Online) $S(q,\omega)$ of gaseous N_2 derived from NIXS (thick line) spectra, EELS (dotted line) spectra, and as predicted by TDLDA (thin line). Spectra are offset for presentation, but otherwise NIXS and TDLDA are normalized to eV^{-1}, as are EELS data, insofar as Eq. (1) holds for the EELS results at a given q.

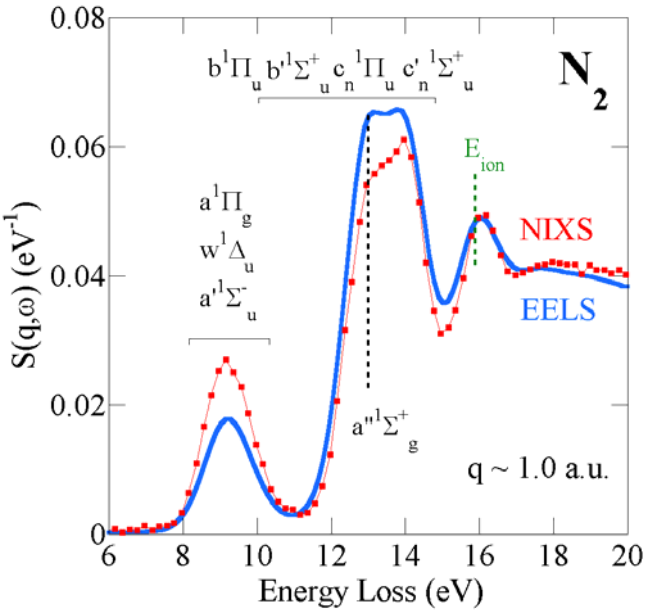

FIG. 3. (Color Online) NIXS (thin line thru points) and EELS (thick solid line) valence excitation spectra of N_2 gas at a single momentum transfer. Known features are labeled by their symmetry designation, and the first ionization energy (E_{ion}) is indicated as well. The Lyman-Birge-Hopfield band centered at ~ 9 eV may contain contributions from the presumed dominant $a^1\Pi_g$ (E = 9.3 eV), the $w^1\Delta_u$ (E = 9.8 eV) and the $a'^1\Sigma_u^-$ (E = 10.2 eV). EELS data is broadened to match NIXS energy resolution.

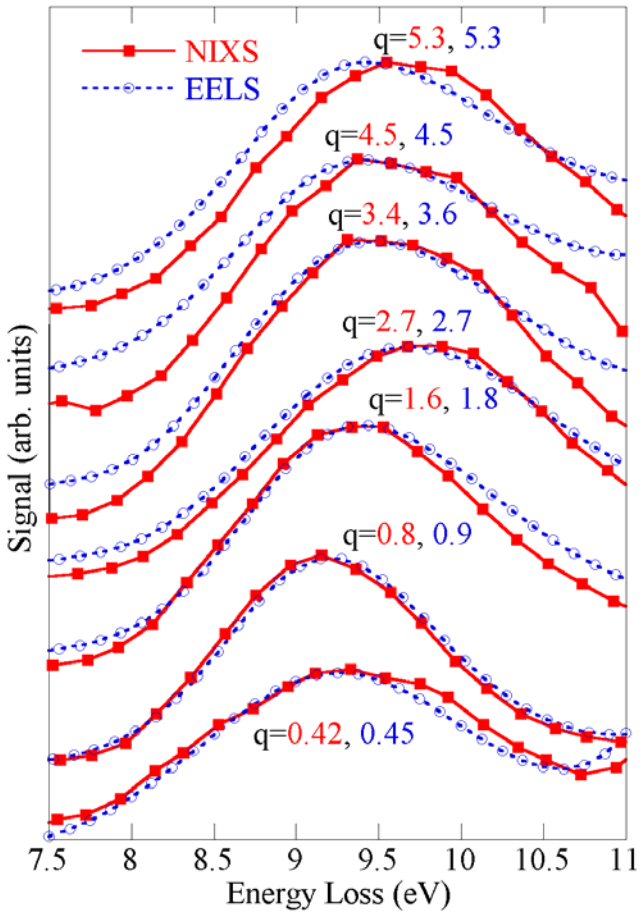

FIG. 4. (Color online) A fine detail view of the NIXS and EELS LBH features. The EELS data is broadened to match NIXS energy resolution, and then multiplicatively scaled to match NIXS intensity. Both data sets are presented *without* removal of the low-energy tails from transitions at 13-15 eV. Removal of these features introduces uncertainty in LBH feature shape, but negligibly affects the LBH peak locations. The dependence of LBH lineshape and peak location on q is direct evidence for contribution from not only the $a^1\Pi_g$ but also the $w^1\Delta_u$ resonance. Momentum transfers listed are in atomic units.

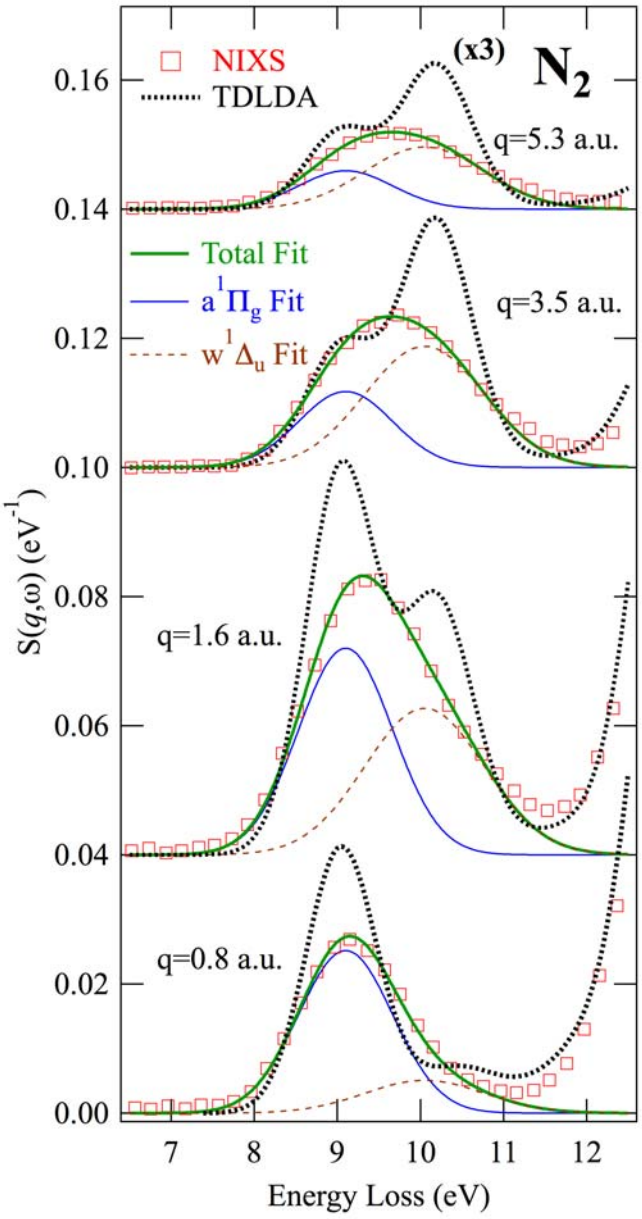

FIG. 5. (Color online) Comparison of NIXS results and TDLDA predictions for the excitation spectrum in the LBH region of N_2. Results of fitting the LBH band with the combination of $a^1\Pi_g$ and $w^1\Delta_u$ features at selected momentum transfers. Solid lines are the fits, and the measured data are in red boxes. Spectra are offset for clarity.

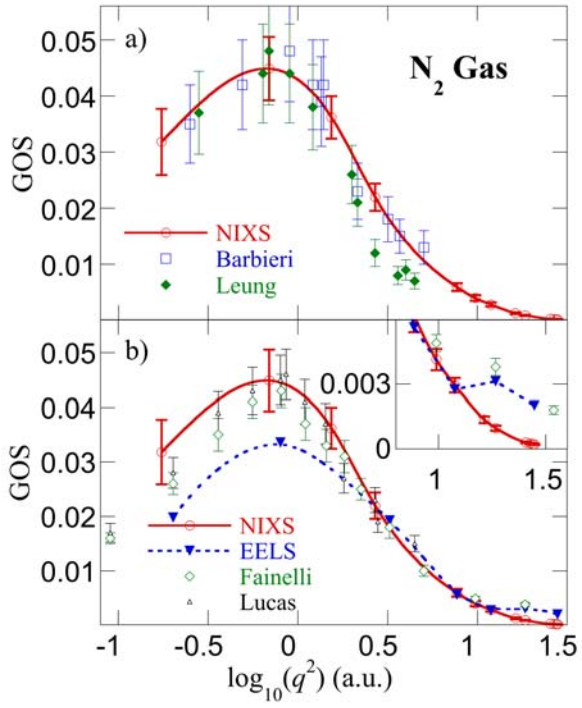

FIG. 6. (Color online) Generalized oscillator strength (GOS) as a function of momentum transfer. 6a) and b) compare NIXS and EELS LBH generalized oscillator strength (GOS) results to previous EELS experiments.

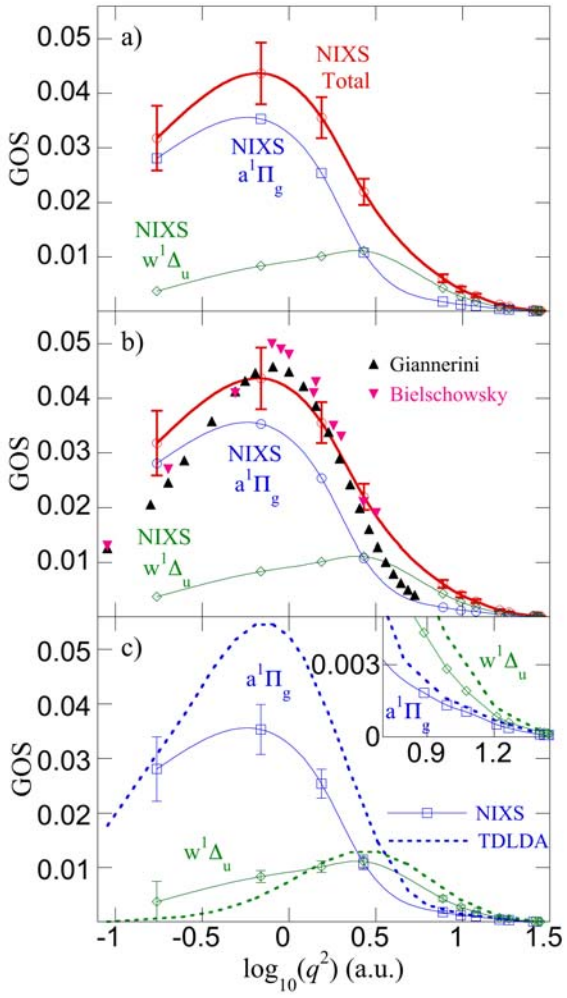

FIG. 7 (Color online) Generalized oscillator strength (GOS) as a function of momentum transfer. Figure a) shows the decomposition of the total LBH band into its two dominant electronic excitations, $a^1\Pi_g$ and $w^1\Delta_u$. Figure b) compares these results with previous theoretical calculations of the $a^1\Pi_g$ feature alone, made using the Born approximation. Figure c) compares the decomposed experimental GOS curves with the two features predicted in the current TDLDA calculation.

1. J. A. Bradley, et al., Phys. Rev. Lett. **105,** 053202 (2010).
2. T. T. Fister, et al., J. Amer. Chem. Soc. **130** (3), 925 (2008).
3. R. A. Gordon, et al., EPL **81** (2), 26004 (2008).
4. W. L. Mao et al., Science, **302,** 425 (2003).
5. S. K. Lee et al., Nature Mat. **4,** 851 (2005).
6. Y. Q. Cai et al., Phys. Rev. Lett., **94,** 025502 (2005)
7. Y. Meng et al., Nature Mat., **3** 111 (2004)
8. A. Lazicki et al., Phys. Rev. Lett. **95** ,165503 (2005)
9. M. Pravica et al., J. Phys. Chem. B, **111,** 11635 (2007)
10. S. K. Lee et al., Proc. Nat. Aca. Sc. **105**, 7925 (2008)
11. H. K. Mao et al., Phys. Rev. Lett. **105** 186404 (2010)
12. C. Sternemann et al., Phys. Rev. B, **72**, 035104 (2005)
13. H. C. Weissker et al., Phys. Rev. B, **81**, 085104 (2010)
14. J. –F. Lin et al., Phys. Rev. B, **75**, 012201 (2007)
15. H. Fukui et al., J. Chem. Phys., **127** (13), 134502 (2007)
16. J. P. Rueff and A. Shukla, Rev. Mod. Phys., **82**, 847 (2010)
17. L. F. Zhu et al., J. Phys. B, **44** (2), 025203 (2011)
18. B. P. Xie et al., Phys. Rev. A, **82,** 032501 (2010)
19. U. Bergmann et al., Phys. Rev. B, **66,** 092107 (2002)
20. K. Hämäläinen et al., Phys. Rev. B **65,** 155111 (2002)
21. M. H. Krisch et al., Phys. Rev. Lett. **78,** (14), 2843 (1997)
22. M. Minzer, et al., Rev. Sci. Instrum. **79,** 086101 (2008).
23. B. P. Xie, et al., Phys. Rev. A, **82,** 032501 (2010).
24. K. P. Nagle, et al., Phys. Rev. B **80,** 045105 (2009).
25. T. T. Fister, et al., J. Chem. Phys. **129,** 044702 (2008).
26. Y. Feng, et al., Phys. Rev. B, **77,** 165202 (2008).
27. A. Sakko, et al., Phys. Rev. B **81,** 205317 (2010).
28. T. Pylkkänen, et al., J. Phys. Chem. B **114,** (41), 13076 (2010).
29. J. A. Bradley, et al., Phys. Rev. B **81,** 193104 (2010).
30. J. A. Bradley, et al., J. Am. Chem. Soc. **132,** (39), 13914 (2010).
31. J. M. Ajello and D. E. Shemansky, J. Geophys. Res. - Space Phys. **90**, 9845 (1985).
32. R. S. Barbieri and R. A. Bonham, Phys. Rev. A **45,** 7929 (1992).
33. M. J. Brunger and P. J. O. Teubner, Phys. Rev. A **41** (3), 1413 (1990).
34. D. C. Cartwright, et al., Phys. Rev. A **16**, 1013 (1977).
35. S. Chung and C. C. Lin, Phys. Rev. A **6,** (3), 988 (1972).
36. E. Fainelli, et al., Nuovo Cimento Della Societa Italiana Di Fisica D-Condensed Matter Atomic Molecular and Chemical Physics Fluids Plasmas Biophysics **9** (1), 33 (1987).
37. Y. Itikawa, et al., J. Phys. Chem. Ref. Data **15** (3), 985 (1986).
38. M. A. Khakoo, et al., Phys. Rev. A **71**, 062703 (2005).
39. E. N. Lassettre and M. E. Krasnow, J. Chem. Phys. **40**, 1248 (1964).
40. E. N. Lassettre, et al., J. Chem. Phys. **42** (2), 807 (1965).
41. K. T. Leung, J. Electron Spectr. Rel. Phenom. **100**, 237 (1999).
42. N. Oda and T. Osawa, J. Phys. B-At. Mol. Opt. **14** (17), L563 (1981).
43. A. Skerbele and E. N. Lassettr, J Chem Phys **53** (10), 3806 (1970).

44. H. F. Wellenstein, et al., Rev Sci Instrum **46** (1), 92 (1975).
45. D. G. Wilden, et al., J Phys B-at Mol Opt **12** (9), 1579 (1979).
46. T. C. Wong, et al., J. Chem. Phys. **63** (4), 1538 (1975).
47. P. V. Johnson, et al., J.Geophys. Res. - Space Physics **110,** (A11) (2005).
48. R. R. Meier, et al., J Geophys Res-Space **85** (Na5), 2177 (1980).
49. D. J. Strickland, et al., J Geophys Res-Space **104** (A3), 4251 (1999).
50. T. Giannerini, et al., Phys. Rev. A **75**, 012706 (2007).
51. A. Szabo and N. S. Ostlund, Chem Phys Lett **17** (2), 163 (1972).
52. G. G. B. deSouza and C. A. Lucas, ICPEAC Book of Abstracts (1985).
53. M. Inokuti, Rev. Mod. Phys. **43,** 297 (1971).
54. T. T. Fister, et al., Rev. Sci. Instrum. **77,** 063901 (2006).
55. H. Sternemann, et al., Journal of Synchrotron Radiation **15,** 162 (2008).
56. R. H. J. Jansen, et al., J. Phys. B: Atom. Molec. Phys. **9,** 185 (1976).
57. M. A. L. Marques, et al., *Time-dependent density functional theory*. (Springer-Verlag, Heidelberg, 2006).
58. A. Castro, et al., Phys. Stat. Sol. B **243,** 2465 (2006).
59. A. Sakko, et al., J. Chem. Phys. **133,** 174111 (2010).
60. M. E. Casida, edited by D. P. Chong (World Scientific, Singapore, 1995).
61. K. Yabana and G. F. Bertsch, Phys. Rev. B **54**, 4484 (1996).
62. T. Nakatsukasa and K. Yabana, J. Chem. Phys. **114** (6), 2550 (2001).
63. Y. Imamura and H. Nakai, Int. J. Quantum Chem. **107** (1), 23 (2007).
64. D. C. Cartwright, et al., Phys. Rev. A **16,** 1041 (1977).
65. J. A. Soininen, et al., Phys. Rev. B **72,** 045136 (2005).
66. M. W. Haverkort, et al., Phys. Rev. Lett. **99,** 257401 (2007).
67. J. A. Soininen, et al., Journal of Physics-Condensed Matter **18** (31), 7327 (2006).
68. A. Lofthus and P. H. Krupenie, J Phys Chem Ref Data **6** (1), 113 (1977).
69. A. Hesselmann and A. Görling, Phys. Rev. Lett. **102,** 233003 (2009)